https://dx.doi.org/10.1016/j.cemconcomp.2022.104655

Mechanism of carbonating recycled concrete fines in aqueous environment: the particle size effect

Yi Jiang[a], Long Li[a], Jian-xin Lu[a], Peiliang Shen[a]*, Tung-Chai Ling[b], Chi Sun Poon[a]*

[a] Department of Civil and Environmental Engineering & Research Centre for Resources Engineering towards Carbon Neutrality, The Hong Kong Polytechnic University, Hong Kong, China

[b] College of Civil Engineering, Hunan University, Changsha 410082, Hunan, China

*Corresponding authors: peiliang.shen@polyu.edu.hk (P.L. Shen), cecspoon@polyu.edu.hk (C.S. Poon)

Abstract

Processing waste concrete in recycling facilities inevitably generates by-products such as very fine particles (<2.36 mm) and powders (<0.15 mm). The resourcing of these low-value recycled concrete fines (RCFs) has attracted increasing interest from the construction industry. This study attempts to elucidate the underlying mechanisms of particle size effects on carbonating RCFs via aqueous route. The results suggested that the relatively coarse particles (0.6-1.18mm and 1.18-2.36 mm) experienced two positive effects i.e., i) improvement of surface properties by the formation of a reactive shell, and ii) significant densification of the microstructure. This was due to an initial carbonation mediated in the bulk solution, and then the internal carbonation due to the inward diffusion of carbonate species. Meanwhile, the finer particles (<0.15 mm) showed significantly different effects i.e., being totally disintegrated and converted to a calcium carbonate and silica gel composite. Such a difference was attributed to the long alkalinity maintaining ability and extensive dissolution and leaching associated with the high fineness. Whereas 0.15-0.6 mm was regarded as a transition particle size where balanced decomposition and densification were observed. Finally, after carbonating for only 6 h, the carbonated RCFs was found to enhance the compressive strength of pastes (as cement substitute) and mortars (as fine aggregate substitute) by an average of 13.2% and 9.0% in comparison with those prepared with raw RCFs.

Keywords: Aqueous carbonation; Recycled concrete fines; Pore structure

1 Introduction

Recycling waste concrete has been the research target over the last decades, and incorporating recycled concrete aggregate (RCA) in new concrete as alternative to natural aggregate is a preferential solution considering its huge accommodation capacity [1]. However, the use of RCA typically results in deterioration of mechanical and durability properties of the resulting concrete as compared with normal concrete, which is critically owing to the residue of cement paste on RCA [2, 3]. The residual cement paste contains microcracks and high porosity as well as creates multiple interfacial transition zones (ITZ). Therefore, the recycling of the coarse RCA is relatively mature as it contains less residual cement paste (<20 wt.% [4, 5]) and is closer to the properties of natural aggregate than their finer counterparts [1]. However, the recycled concrete fines (RCF) including both the fine aggregates and powders typically have 20-50 wt.% residual cement paste, demonstrating a more detrimental effect on the properties of new concrete [6]. The drawback of utilizing the fine aggregates was that they contained more microcracks and higher porosity [1], while that of utilizing the powders was that they already lost cementing abilities owing to the hydration history, resulting in the dilution of binders [7, 8]. Different approaches aiming at improving the quality of RCA and RCF were proposed including (i) removing the residual cement paste by acid dissolution, mechanical grinding etc., and (ii) strengthening the residual cement paste using polymer emulsion, pozzolan slurry and sodium silicate, etc. [9, 10]. However, these treatments were either energy- or cost- intensive; thus the accelerated carbonation became preferred among these methods [11-13].

Gas-solid accelerated carbonation is one of the effective carbonation routes and it is applied by exposing the RCA/RCF to CO_2-rich gaseous environment. The reaction between calcium phases and CO_2 could induce the precipitation of calcium carbonate (Cc) inside the aggregate and thus reduce its porosity [11, 14]. As such, decrease of water absorption and crushing value by 1.3-29.0% and 7.6-25.9% respectively, as well as an increase in the density by 0.2-5.6% could be obtained [11, 13, 15, 16]. Moreover, the use of carbonated aggregate could significantly improve the mechanical and durability properties of the resulting new concrete [2, 13-17]. Also, gas-solid carbonation was found to be feasible to activate the reactivity of waste concrete powders [18] for its potential application as supplementary cementitious materials (SCMs) [19-21]. As exemplified in the work of [18, 19], the carbonated powders were able to replace 20% cement to attain up to 22% strength increase. Nevertheless, most of the previous studies

reported that both the internal moisture of the materials and the relative humidity (RH) of the carbonation environment should be carefully regulated during the carbonation to create a favourable condition for CO_2 diffusion. It was because CO_2 gas diffusion was the rate-limiting step and depended heavily on the availability of diffusion paths (i.e., the connected pores) [22-24]. The gradually limited mass transport of CO_2 to the reactive sites of carbonation imposed a critical barrier to achieving high carbonation degree.

Aqueous carbonation (AC) is a different carbonation route based on liquid-solid reactions [25-27]. It is conducted by immersing the solid materials in a bulk liquid (i.e., at high liquid to solid ratios) and injecting CO_2. The gaseous CO_2 is transformed into aqueous carbonate species (i.e., CO_3^{2-} and HCO_3^-) upon contact with the bulk liquid before its diffusion to reaction sites. Several previous studies have investigated the differences of AC and gas-solid carbonation based on alkaline wastes [27-29]. It was highlighted by Kashef-Haghighi et al. [28] and Faraji et al. [30] that the aqueous system didn't present interparticle voids and the bulk liquid could saturate the internal pores; thus, a higher surface area could be exposed to the dissolved CO_2. Besides, according to Le Chatelier's principle, the CO_2 dissolution could be favored in highly alkaline aqueous environment, thus increasing the CO_3^{2-} availability [31], and in the meantime the CO_2 dissolution could cause the enhanced dissolution of calcium because of the solution neutralization. With the above characteristics, Ghacham et al. [29] and Liu et al. [26] reported that AC had a higher carbonation efficiency than gas-solid carbonation. However, both the diffusion and dissolution were particle size dependent [30]; hence different size fractions of RCFs were believed to have significantly different responses towards AC. Experimental findings from Zajac et al. [25] and Shen et al. [32] suggested that AC was highly efficient in decomposing RCF powders and converting them to good-quality SCMs. Conversely, Liu et al. [26] obtained a densified RCF microstructure after subjecting to AC. This decomposition-densification discrepancy and the lack of knowledge could significantly affect the RCF reclamations. There are no systematic studies identifying the exact influences of AC on RCFs and particularly its particle size effect. Therefore, finding the linkage among the microstructural modifications of different particle sizes could promote the understanding and applications of AC.

This study attempts to systematically evaluate the influences of AC on RCFs with different particle sizes (i.e., 1.18-2.36mm, 0.6-1.18mm, 0.15-0.6mm and <0.15mm). The changes of the two constituents

in RCFs (i.e., cement paste and inert phases) in terms of phase assemblages, microstructures and surface morphologies were comprehensively characterized and studied. Meanwhile, the CO_2-water-RCFs interactions in terms of pH, electrical conductivity (EC) and elemental concentrations to reveal the reaction kinetics were presented and discussed. Moreover, the performance of carbonated RCFs in new pastes/mortars was demonstrated.

2 Materials and methods

2.1 Materials

The changes of residual cement paste were investigated based on modelled RCFs derived from laboratory-prepared cement paste. For the purpose of examining the CO_2-water-RCFs interactions, the same modelled RCFs were used, and then the results were validated using real RCFs obtained from waste concrete. Subsequently, the influence of AC on inert phases and the applications of RCFs in new paste/mortar were evaluated only with real RCFs.

Specifically, laboratory-prepared cement paste was made by mixing ordinary Portland cement (CEM I 52.5N as per BS EN197-1:2000) and water at a water to cement ratio of 0.45 and cured in sealed bags at ambient temperature for over seven months. While the waste concrete was collected from a demolition site in Hong Kong, in which granite and quartz sand were used as the original natural aggregate. The chemical and mineralogical compositions of the two materials, as determined by X-ray fluorescence and X-ray diffraction, are shown in Table 1 and Fig. 1 respectively, indicating that the waste concrete contained less CaO, more SiO_2 and alkali than the pure cement paste due to the incorporation of natural aggregate (quartz, albite and microcline).

Table 1. Chemical compositions of the waste concrete and cement paste (wt.%).

	CaO	SiO_2	Al_2O_3	Fe_2O_3	Na_2O	K_2O	MgO	Others
Waste concrete	27.8	51.8	9.5	2.1	2.0	3.7	0.9	2.2
Cement paste	66.9	19.8	5.1	3.6	/	0.5	0.9	3.2

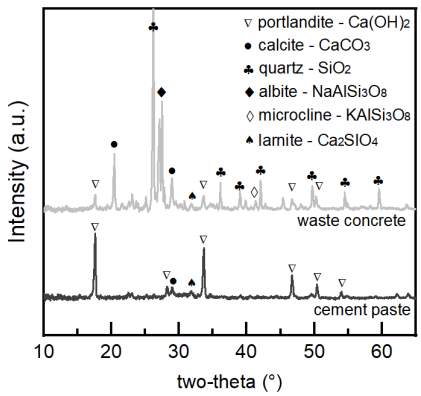

Fig. 1. Mineralogical compositions of the waste concrete and cement paste.

To obtain different size fractions of RCFs, both the cement paste and the waste concrete were crushed and sieved to four different fine fractions (i.e., 1.18-2.36mm, 0.6-1.18mm, 0.15-0.6mm, and <0.15mm) that notated as RCF236, RCF118, RCF060 and RCF015 respectively, as shown in Fig. 2. The residual cement paste content in the real RCFs was determined using the hydrochloric acid (HCl) dissolution method. Specifically, the RCFs were soaked in 0.1M HCl solutions at 25°C and stirred for 24h [33, 34]. Then, the remaining solids were washed with deionized water and dried in oven until constant weight. The final mass loss in the percentage of initial mass was determined as the residual cement paste content. The results shown in Table 2 suggested that the real RCFs contained 32.26-50.41 wt.% residual cement paste and the percentage increased with decreasing particle size.

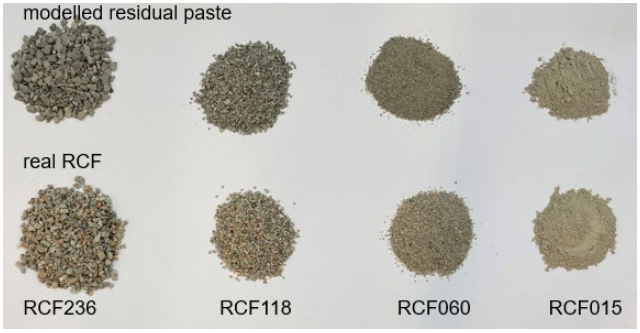

Fig.2. Physical appearance of the real RCFs and the modelled RCFs.

Table 2. Amount of residual cement paste and inert phases in real RCFs (wt.%).

	RCF015	RCF060	RCF118	RCF236
Residual cement paste	50.41	39.92	36.34	32.26
Inert phases (i.e., quartz and granite)	49.59	60.08	63.66	66.74

2.2 Aqueous carbonation

AC was conducted using the laboratory setup shown in Fig. 3. Deionized water was used as the initial liquid and designated amounts of RCFs were added to keep a water to solid ratio of 10 (see Table 3). The reaction temperature was controlled constantly at 25 °C by a water bath, and smooth agitation was applied by magnetic stirring at 500 revolutions per minute. The RCFs were pre-soaked in water for 15 min before the start of carbonation reaction aiming to obtain an initial dissolution equilibrium. Subsequently, the carbonation experiment was carried out for up to 6h by injecting CO_2 gas (99.8 vol.% purity) into the solution via a diffuser at 10 mL/(g·min) as controlled by a flow meter (MFC 8713, Burkert). During carbonation, the pH and EC were constantly recorded by a pH meter (HM-30P, DKK-TOA) and an EC meter (DDSJ-318, Rex). Meanwhile, the solution and RCFs were sampled from the reacting system at different intervals for further analyses until the end of the carbonation (i.e., 6 h).

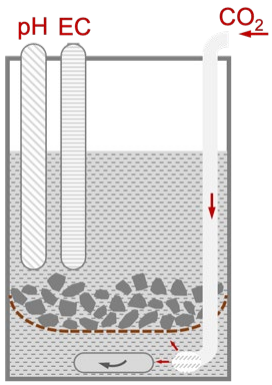

Fig. 3. Laboratory setup for aqueous carbonation.

Table 3. Experimental groups for AC

No.	Materials (g)				Water (mL)	Gas flow rate (mL/min)
	RCF236	RCF118	RCF060	RCF015		
1	40		/	/	400	400
2	/	40	/	/		
3	/		40			
4	/		/	40		

2.3 Testing methods

2.3.1 Thermogravimetric analysis (TGA)

TGA was used to determine the amount of portlandite (CH) and calcium carbonate (Cc) formed in carbonated cement paste. Before the test, the collected samples were soaked in isopropanol for two days and dried in a vacuum desiccator for another two days to remove the free water. TGA was conducted using Rigaku 8121 on 13.0 mg ground materials in an argon atmosphere at a heating rate of 10 °C/min from room temperature to 1000 °C. Quantification of CH and Cc was performed as per the integration method introduced in [35, 36]. Specifically, the amount of CH/Cc is equivalent to the integration of its peak area in the derivative thermogravimetric (DTG) curve as illustrated in the following Fig. 4, and then the results were normalized either to the clinker phase or to the initial sample mass following Eq. 1.

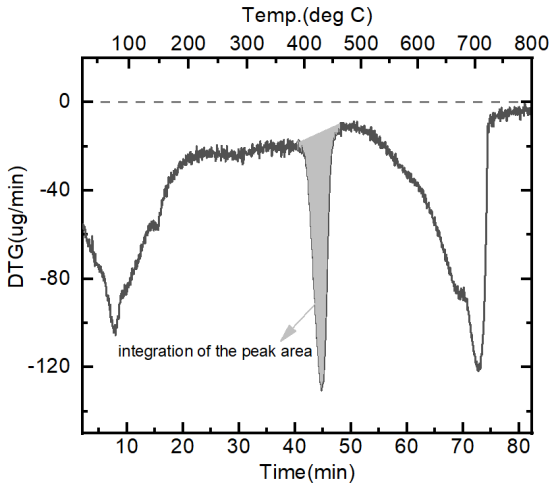

Fig. 4. Illustration for the integration method.

$$P_p(\%)=\frac{m_g \times M_P}{M_g \times m_{initial/1000°C}} \times 100=\frac{A_g \times M_P}{M_g \times m_{initial/1000°C}} \times 100 \quad (1)$$

Where P_p is the weight percentage of the CH/Cc to be determined, m_g is the mass of the H_2O/CO_2 from CH/Cc decomposition, Mg is the molar mass of H_2O/CO_2 and MP is the molar mass of CH/Cc, $m_{initial}$ is the initial dry mass of the sample, m1000°C is the mass of sample at 1000°C from TGA measurement, A_p is the integration of the peak area of H_2O/CO_2.

2.3.2 X-ray diffraction (XRD)

XRD was performed on a Rigaku Smartlab 9kW diffractometer using Cu Kα at 45kV and 200mA. The spectra were obtained with the 2θ of 5-60°, at a step size of 0.02° and 5°/min.

2.3.3 Magic angle spinning nuclear magnetic resonance (MAS NMR)

^{29}Si MAS NMR spectra were collected using a JEOL JNM-ECZ500R/S1 spectrometer, operating at a Larmor frequency of 98.4 MHz (magnetic field strength= 11.6 T). Dried samples were ground, loaded and packed into 8mm zirconia rotors and scanned with the spinning frequency of 4 kHz and the relaxation delay of 30 s.

2.3.4 Scanning electronic microscopy (SEM)

For microstructure investigation, a TESCAN VEGA3 scanning electronic microscope (SEM) equipped with an energy-dispersive X-ray spectroscope (EDS) was used. Secondary electron (SE) imaging was performed directly on dried and gold-coated samples to observe the surface morphologies. Backscattered electron (BSE) imaging was performed on polished epoxy-impregnated samples. For RCF015, the powder was firstly pre-pressed into a tablet under 30 kN and then the tablet was impregnated in epoxy resin, followed by grinding with P1200 abrasive paper and polishing with 9um/3um/0.05um diamond/alumina sprays. For RCF060 to RCF236, the particles were solely impregnated in epoxy and followed by the same grinding and polishing procedures.

2.3.5 Nitrogen adsorption-desorption

Brunauer-Emmett-Teller (BET) Nitrogen adsorption-desorption test was carried out with a Micromeritics ASAP2020 PLUS to determine the pore volume and pore size distribution of the cement paste. Prior to the measurements, the samples were degassed at 60 °C for 12 h and Barrett-Joyner-Halenda (BJH) adsorption branch of the isotherm was used for data extraction.

2.3.6 Inductively coupled plasma-optical emission spectrometry (ICP-OES)

ICP – OES was used to determine the concentrations of major elements (e.g., Ca, Si, Al, S, Na and K) in the solutions collected at different carbonation intervals. Pre-treatments of the solutions included i) filtration through 0.45 μm membrane filters, ii) digestion in concentrated nitric acid, iii) re-dissolution of the solid residues after digestion by diluted nitric acid back to the original volume and iv) dilution of the samples. Standard solutions containing Ca, Si, Al, S, Na and K were prepared which concentrated

at 0.01, 0.05, 0.1, 0.2, 0.5, 1, 2, 5, and 10 mg/L. Three measurements were performed for each sample and quality control was conducted for every 30 samples with 2 mg/L standard.

2.3.7 Water absorption

The water absorption of RCFs was determined as per the procedures prescribed in ASTM C128. Prior to the test, the RCFs were immersed in water for 24 h. Approximately 500 g RCFs were obtained and then they were dried at 60 °C in ventilated oven for 2 days. The mass difference between SSD and oven dried RCFs were divided by the dried mass to obtain the water absorption.

2.3.8 Compressive strength

Mortar samples were prepared with natural river sand and SSD real RCFs (including RCF060, RCF118 and RCF236). The weight ratio of aggregate: cement: water was controlled at 2:1:0.45. The natural sand was replaced by raw/carbonated RCFs at 20%, 40% and 60% and the slump flow of all the mixes were 210±10 mm. Meanwhile, paste samples were prepared by using RCF015 as the cement replacement at 10%, 30% and 50% and the water to cementitious materials ratio was controlled at 0.5. The mortar and paste samples were cast into 40 mm and 20 mm cubic molds respectively, and after demolding, they were cured in saturated lime water for 28 days prior to the compressive strength tests and an average strength from 5 samples for each group was reported.

3 Results and discussion

3.1 Influence of AC on phase evolution of RCFs

3.1.1 Precipitation of Cc as a function of particle size

Cc is the major product of RCF carbonation. The amount of Cc generated versus the particle size and carbonation time is presented in Fig. 5. Given that 3.2% Cc was originally contained in the raw RCF by weight of the clinker phase, it drastically increased to 46.9% for RCF015 after carbonation for just 10 min, and to 62.5% after 30 min. Thereafter, the precipitation rate became much less significant and reached a plateau at about 1 h. The final amount of Cc was determined as 70.7%. Upon the increase of particle size as in the cases of RCF060, RCF118 and RCF236, the Cc amounts were increased to 14.6%, 11.1% and 7.4% respectively after 30 min and reached the final values of 21.5%, 14.2% and 9.0%

respectively. This trend indicated that Cc precipitation was very intensive regardless of the particle size, as 68-88% of the final amount of Cc was formed within 30 min. However, the total amount of Cc depended heavily on particle size: finer particles obtained much higher amount of Cc than their coarse counterparts. From the composition perspective, RCF015 was significantly transformed into a Cc composite [37]. Based on the XRD patterns as shown in Fig. 6, the precipitated Cc was confirmed as calcite and the presence of other polymorphs such as aragonite and vaterite was not detected. The Cc content in real RCF060 was also determined for comparison. It was found that 6.7% calcite by weight of the initial sample mass was included in the raw sample. This was due to the natural weathering process either in its service life, or in the sample collection, crushing and handling processes. Despite the high initial Cc amount, the Cc evolution followed a similar trend with the paste RCFs after AC, with the final Cc accounting for 15.1%.

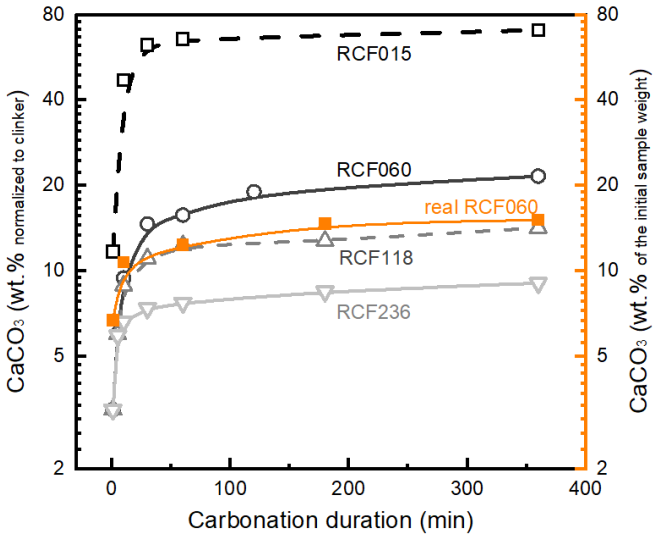

Fig. 5. Development of Cc amount as a function of time in different sizes of RCFs.

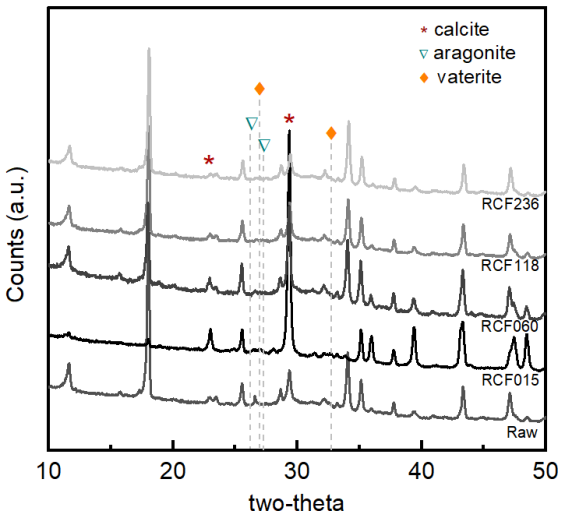

Fig. 6. XRD patterns of the raw and carbonated RCFs.

Cc generated at the expense of either pure calcium-bearing phases (i.e., CH) or calcium- and silicon-bearing phases (e.g., C-S-H, ettringite, AFm, anhydrous phases). Identifying the source of calcium in Cc could promote the understanding on the solid dissolution behaviour in the bulk solution. To this end, the amount of CH consumption and the Cc formation between two different carbonation durations (i.e., 10 min, 30 min, 60 min, 360 min) were calculated based on TG results, with their difference being assigned to the molar amount of Ca originated from other hydration products (represented by C-S-H herein). A factor α was designated to measure the molar ratio of calcium from C-S-H to the calcium from CH.

As shown in Fig. 7, after carbonating for 10 min, the α value for RCF015 was 1.3, indicating that the Cc originated from both C-S-H and C-H, with the former accounting for more than 50%. Typically from a thermodynamic viewpoint, decalcification of C-S-H was believed to take place after the depletion of CH [38]. However, the net CH consumption was still increasing which reflected its availability at 10 min. Therefore, it is believed that C-S-H phase participated in carbonation earlier than expected. This might be critically attributed to the presence of the bulk solution that significantly diluted the elemental concentrations, which resulted in the greater undersaturation and thus the earlier dissolution of C-S-H phase [39, 40]. After carbonating for 30 min, the calcium consumption from CH was no longer increased, implying it was locally depleted. Therefore, the formation of Cc relied on consuming the C-S-H.

With the increase of particle size, it was found that the total molar amount of calcium significantly decreased and the α value increased. This reflected the reduced Cc formation and its increasing dependency on C-S-H. This should be explained that the increasing particle size created enlarged physical barriers, and thus the availability of inner CH was much more difficult. With the constant injection of CO_2, the carbonation became more concentrated on the surface layers, which not only consumed all local CH but also more significantly decalcified the C-S-H.

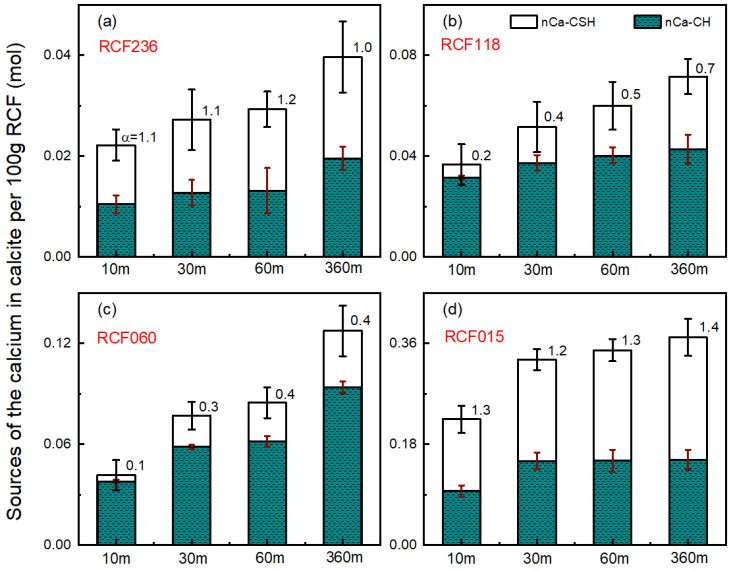

Fig. 7. Sources of the calcium of the precipitated Cc in 100g RCFs where α indicates the molar ratio of calcium from C-S-H to CH.

3.1.2 Formation of silica gel as a function of particle size

After being decalcified, the silicate in the C-S-H started to polymerize and form silica gel. Therefore, the evolution of silicate phases was investigated via ^{29}Si NMR. As depicted in Fig. 8, there are five major resonances and their assignments were given by the annotation in the previous study [41]. The single peak located at 74ppm corresponded to the Q^0 species i.e., the anhydrous silicate minerals. The second and third peaks, which were identified as the silicate dimers (Q^1, 82.6ppm) and chains (Q^2, 87.2ppm) in the C-S-H structure, were observed as the major peaks. In the case of RCF015, upon the initial carbonation within 30 min, the proportion of Q^1 was found to be dramatically decreased (from ~26.7% to ~15.5%), suggesting the obvious polymerization of the dimeric silicate units to Q^2 and even Q^3 species. While the resonances were markedly shifted from Q^2 to Q^3 at 101.1ppm and Q^4 at 109.6ppm (condensed SiO_4 tetrahedra) until carbonation for 1 h. After carbonating for 6 h, about 69.5% of the

265 silica-bearing phases were transformed into silica gel. Unlike the intensive formation of Cc within the
266 30 min, only ~22% of the final amount of silica gel was formed over the same period. Therefore, the
267 formation of silica gel (Q^3 and Q^4) was much slower [25]; it was believed that the difference in the
268 speed of Cc and silica gel formation was mainly due to the availability of calcium and silicon because
269 the dissolution of calcium phases was quick and it existed as Ca^{2+} in the solution while silicon was
270 mostly likely to stay in the chain structure of C-S-H and barely leached into the solution (to be discussed
271 in section 3.3). Therefore, the carbonate ions could react with the Ca^{2+} readily dissolved in the solution.
272 Whereas Si polymerization was only triggered until the complete removal of the interlayer Ca in C-S-
273 H (approx. at a Ca/Si ratio of 1.2) according to [42].

274 Besides, it was determined that RCF060 obtained 17.0% silica gel after carbonation for 6 h while
275 RCF118 and RCF236 obtained only 11.7% and 7.3% respectively, which were significantly lower than
276 the 69.5% of RCF015. As seen in Fig. 8, despite the less formation of silica gel, the Q^4/Q^3 ratio of
277 RCF236 was obviously higher than RCF118, RCF060 and RCF015, suggesting a higher polymerization
278 degree and thus confirming the more thorough decalcification and polymerization of the C-S-H in the
279 surface layer, in line with the conclusion obtained from Fig. 7.

280 Phase evolution implied the changes of reactivity. As discussed above, the RCF015 was totally re-
281 activated via AC into a Cc-silica gel composite, possessing a promising application as SCM. Meanwhile,
282 the RCF060-RCF236 was activated more on the surface layer, thus assumed to have a reactive surface.

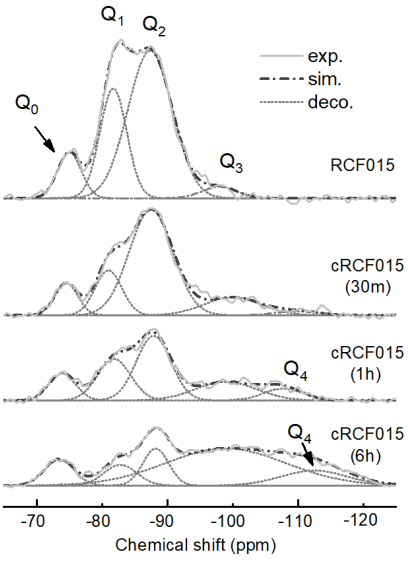

(a)

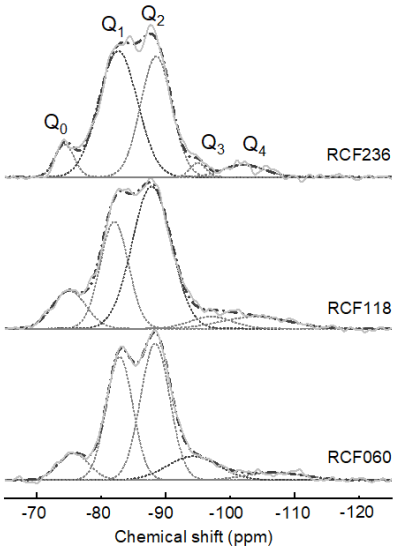

(b)

Fig. 8. 29Si NMR spectra of (a) raw RCF015 and carbonated RCF015 (for different carbonation durations) and (b) carbonated RCF060, RCF118 and RCF236 (for 6 h).

3.2 Influence of AC on microstructure evolution of RCFs

3.2.1 Pore structure and water absorption evolution as a function of particle size

Fig. 9 shows the cumulative pore volume changes for different RCFs upon carbonation. A strong particle size dependent behaviour was observed. The total pore volume of RCF015 was found to markedly increase with time, from the initial 0.104 cm^3/g to 0.177 cm^3/g after 6 h carbonation, indicating a 70% increment. Meanwhile, for RCF060, despite a slight increase within the first hour, the pore volume decreased thereafter, showing ~4% overall increment. As a strong contrast, the pore volume of RCF118 and RCF236 had significantly decreased, from 0.134 cm^3/g to 0.092 cm^3/g and from 0.117 cm^3/g to 0.088 cm^3/g respectively after carbonating for the same duration.

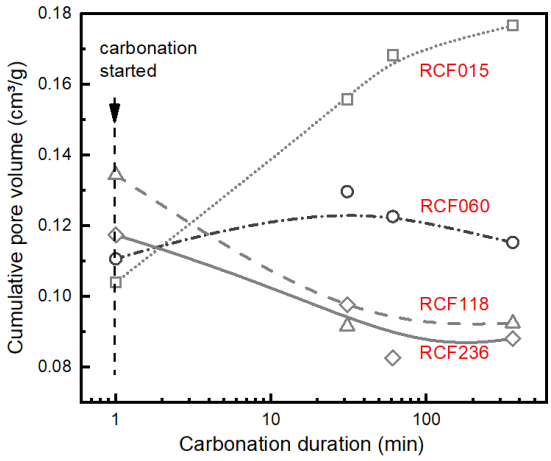

Fig. 9. Cumulative pore volume of RCFs at different carbonation timeslots.

Different from the gas-solid carbonation after which the pore volume was decreased regardless of the particle sizes [14, 43], the particle-size dependency of AC was due to the dissolution and diffusion characteristics in the presence of bulk solution. To reflect the pore size change, the pores were divided into i) gel pores (i.e., diameter=2-10 nm), ii) medium capillary pores (i.e., 10-42 nm) and iii) larger capillary pores (>42 nm) [44, 45]. The results in Fig. 10a and b indicated that RCF015 formed an extensive number of new pores upon contact with water and within the first 30 min. These pores were mostly medium and larger capillary pores that were created due to the massive dissolution of RCF015

304 through capillary channels. Whereas it was noticed that the increase of capillary pores gradually
305 suspended after 30 min and the number of gel pores was notably increased instead. This phenomenon
306 occurred simultaneously with the formation of silica gel (see Fig. 8) and was attributed to the gel pores
307 embedded in the newly formed silica gel. The overall increase in both the capillary and gel pores caused
308 the increase in cumulative pore volume.

309 Comparing the pore size distributions and evolution of RCF118 and RCF236 with RCF015 (see Fig. 10
310 e-h), the increase of capillary pores was found rather limited, demonstrating a restrained solid
311 dissolution relative to RCF015 due to the increase of particle size. Instead, significant pore reduction
312 was obtained. This could be explained by the predominance of carbonate diffusion into the solid matrix
313 over solid dissolution and leaching into the solution. In other words, the carbonation was driven by the
314 internal diffusion of aqueous carbonate species into the solid matrix, thus precipitating the Cc locally
315 and densifying the structure. As for RCF060 (see Fig. 10 c-d), an increase in capillary pores was
316 observed at the initial period which suggested the partial dissolution, but it was reduced afterwards.
317 This was owing to the coupling effect of the initial dissolution and then the extensive internal
318 precipitation of Cc, thus leading to an almost unaltered pore structure. In this regard, RCF060 was
319 considered as the transition particle size below which total decomposition occurred and above which
320 structure densification took place.

321

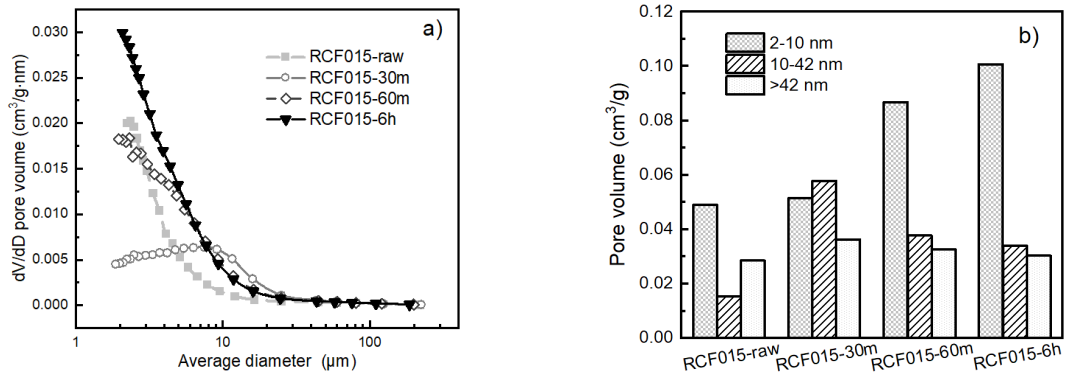

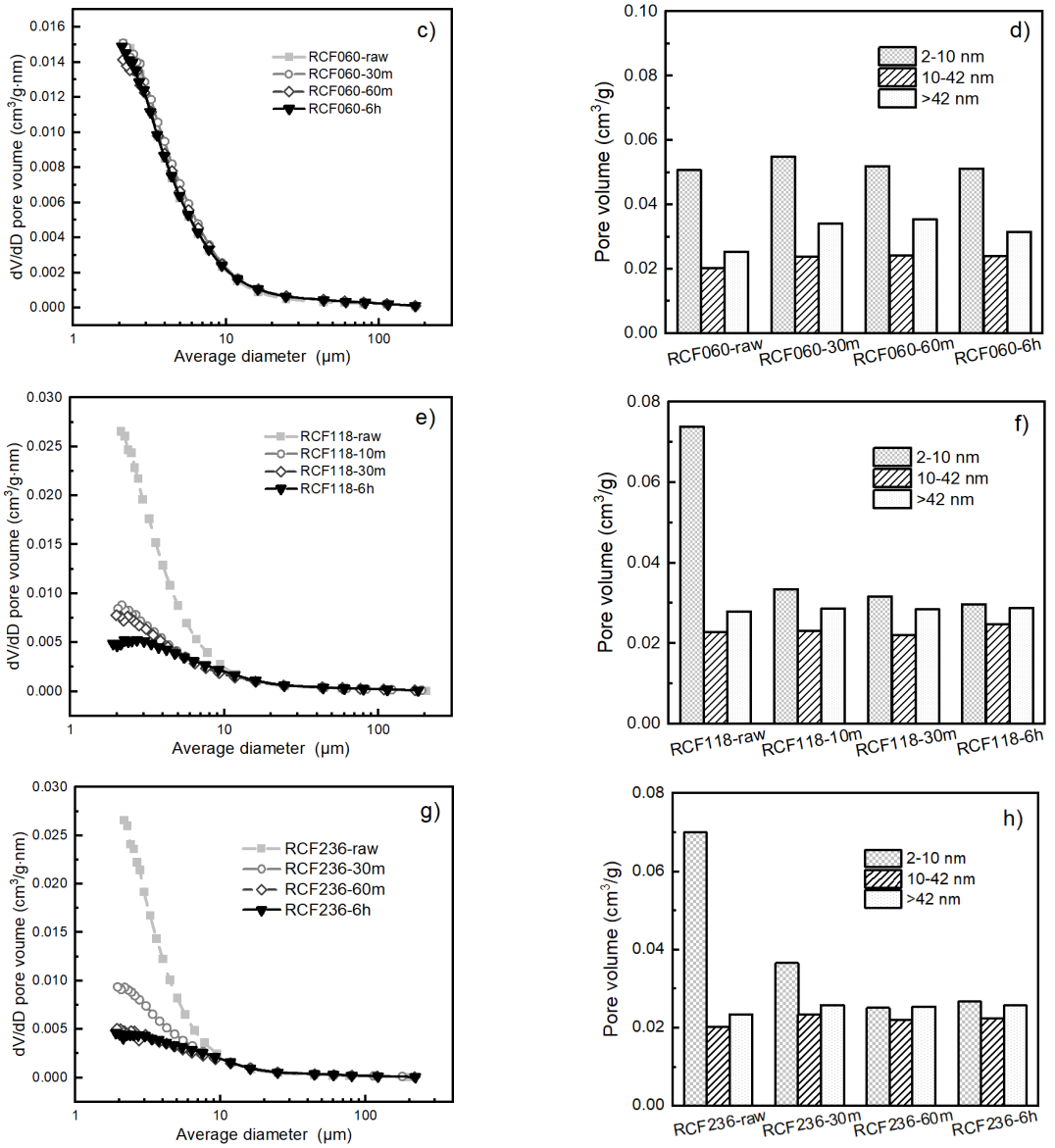

322 Fig. 10. Pore volumes and pore distributions of the (a)(b) RCF015, (c)(d) RCF060, (e)(f) RCF118 and
323 (g)(h) RCF236.

324 The modification of pore structure directly affected the capacity of RCFs to absorb water. Therefore,
325 the water absorption values of RCF060, RCF118 and RCF236 were determined (Table 4). The moisture
326 present in the SSD RCF060 was slightly increased by 0.9% after carbonation for 30 min and then it
327 decreased very slightly after 6 h, consistent with the results of pore structure evolution. Meanwhile, the
328 water absorption values of RCF118 and RCF236 were decreased by up to 1.3%, in good agreement
329 with the changes reported for the matrix densification.

330 Table 4. Water absorption capacity of raw and carbonated RCFs (wt.%).

Groups	raw	Carbonated

			30 min	6h
Water absorption value at 24h	RCF060	23.1±2.1	24.0±1.3	22.5±1.9
	RCF118	15.5 ±0.5	15.1 ±1.0	14.2 ±1.0
	RCF236	13.9 ±0.9	14.0 ±0.7	13.1 ±0.3

3.2.2 Phase distribution

RCF015 was almost totally disintegrated and converted to a Cc and silica gel composite based on the TGA, NMR and BET results. Observations from BSE image and the corresponding EDS mapping were used to corroborate this finding. It can be seen from Fig. 11a that several phases were present, primarily including i) extensive clusters of small grains, ii) some relatively big particles with rims in higher brightness, iii) some cohesive agglomerates and iv) some particles in very high brightness. As annotated in Fig. 11b, the purple, green and yellow colours represented the Si, Al and Ca respectively. It can be clearly seen that the clusters distributed all over the cross-section were coloured in pure yellow and thus recognized as Cc. Meanwhile, the agglomerates were coloured in pure purple, indicating itself as polymerized silica gel. The relatively intact particles and their surrounding rims, coloured in purple and yellow respectively, were believed as the decalcified hydration products and Cc respectively. Besides, those phases with very high brightness and contrast were filled with green or a mix of yellow and purple colours, demonstrating that they were anhydrous calcium aluminates and silicates respectively, consistent with the NMR result. Overall, it can be concluded that RCF015 underwent significant decomposition, with calcium significantly extracted and silicate polymerized. An extensive amount of Cc particles could be observed in the SE image (Fig. 12), and they were distributed everywhere as isolated particles as well as in clusters. Meanwhile, the other materials with fluffy morphologies were believed to be silica gel agglomerated with Cc. Generally, it was verified by SEM that the RCF015 was almost totally decomposed and restructured due to the extensive formation of silica gel and Cc.

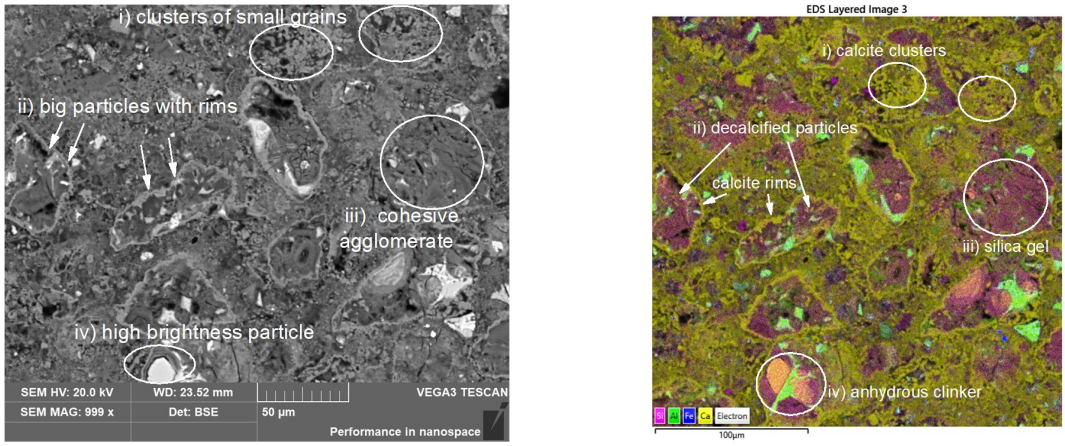

(a) (b)

351 Fig. 11. (a) the BSE image and (b) EDS mapping of carbonated RCF015 tablet.

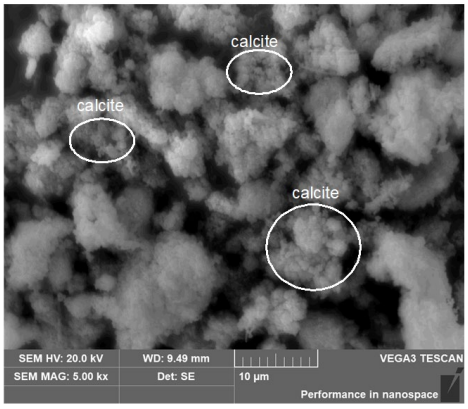

352

353 Fig. 12. SE image of the carbonated RCF015 powder.

354 However, RCF060, RCF118 and RCF236 were modified otherwise as shown in Fig. 13 and they were
355 found to retain their original structures after 6 h carbonation. For the uncarbonated RCF particles (Fig.
356 13a), the edge was sharp and clean, indicating the homogeneity of the outer and the inner matrix.
357 However, after AC, all these RCFs formed an outer layer, exhibiting an obvious shell-core structure.
358 As observed from the SE images (Fig. 14), the surface of carbonated RCF was covered by an extensive
359 network of well-crystallized rhombohedral calcite. Therefore, the outermost layer was found as a Cc
360 coating. This was owing to the dissolution of Ca^{2+} in the bulk solution and the precipitation of Cc on
361 the surface of RCFs. However, slight differences can be observed among particles with different particle
362 sizes. Specifically, the coating of RCF060 was relatively thin and loose, with considerable small Cc
363 grains/clusters distributed outside the matrix, indicating the leaching of calcium and precipitation of Cc
364 in the solution instead of purely on the surface of RCF. This phenomenon, in another perspective, can
365 be regarded as the partial decomposition of the surface layers of RCF060. Meanwhile, for RCF118 and

RCF236, the Cc coatings were thicker and denser. This was because the bigger particle size reduced the contact surface area of the solids with the bulk solution and the dissolution and leaching were considerably decreased. As inferred from pore structure evolution, after the initial formation of Cc layer, carbonation proceeded mostly by the inward diffusion of carbonate species into the RCF matrix and the precipitation occurred gradually inside the solid, thus densifying both the coating and matrix. Moreover, the TGA and NMR also indicated that decalcification and polymerization on the surface layer were more thorough; therefore silica gel layer also existed underneath the Cc coating, together of them forming a reactive shell on the relatively large particles which was previously validated by our previous study [40].

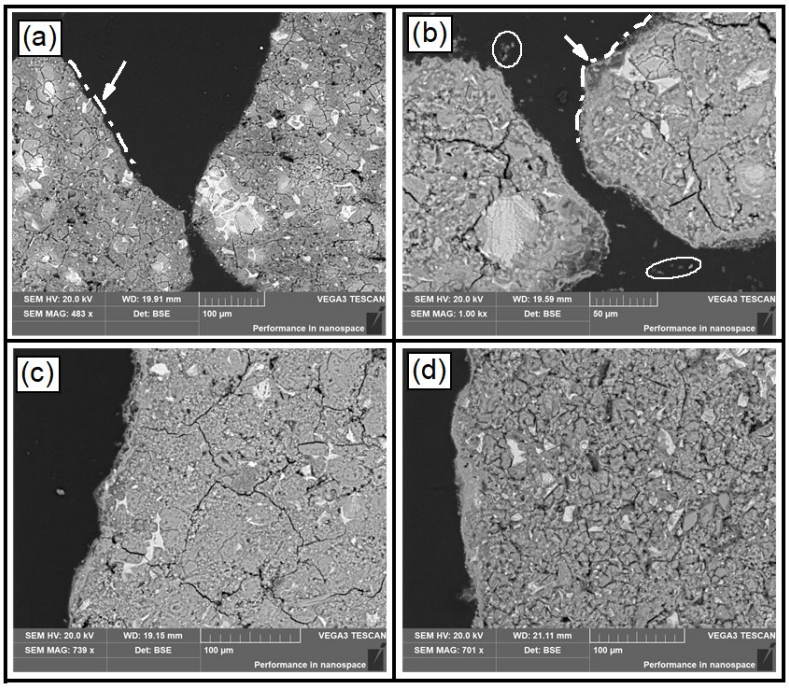

Fig. 13. BSE images of (a) raw RCF060, (b) carbonated RCF060, (c) carbonated RCF118 and (d) carbonated RCF236 particles.

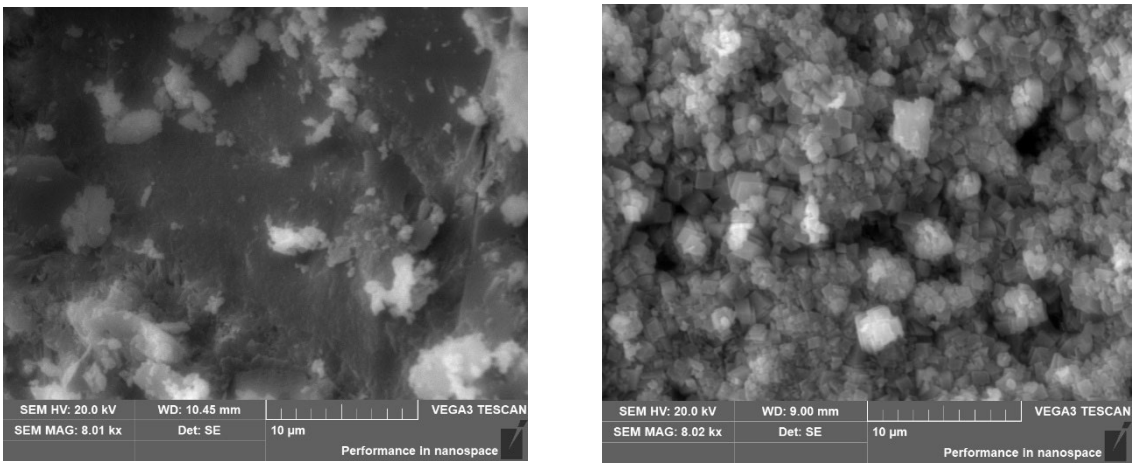

(a) (b)

379 Fig. 14. Surface morphology of the raw RCF and carbonated RCF.

380

381 **3.3 Solution chemistry of CO_2-water-RCFs interactions**

382 The phase and microstructure evolution of RCFs were directly resulted from the characteristic CO_2-
383 water-RCFs interactions due to the use of bulk water and injecting CO_2. Therefore, the reaction kinetics
384 as revealed by pH, EC, and elemental concentrations were discussed.

385 **3.3.1 pH and electrical conductivity**

386 RCFs were alkaline materials due to the incorporation of CH and C-S-H [38]. When the solids were
387 immersed in water, the pH immediately increased. As shown in Fig. 15a, the initial pH for RCF015,
388 RCF060, RCF118, and RCF236 were 13.26, 13.21, 12.58 and 12.39 respectively, indicating the similar
389 and high alkaline nature of the four water-RCF systems. As carbonation started by injecting CO_2, the
390 alkalinity decreased due to the consumption of OH^- by H^+ as speciated after the dissolution of CO_2 i.e.,
391 the neutralization process. By comparing the data, a critical difference was observed i.e., the time
392 reaching neutrality. As can be seen, pH sharply decreased in terms of RCF236, RCF118 and RCF060;
393 only 2-6 min was required to reach a pH value of 7. However, the pH decrease in the case of RCF015
394 was significantly buffered and an extensively longer time (~23 min) was needed to reach neutrality.
395 Subsequently, the bulk solution became acidic (pH<7) and the rate of pH changes was found to
396 significantly slow down, reaching the minimum values (pH=6.01-6.63) at around 30 min regardless of
397 the particle sizes and then showing very slow and slight pH rebound afterwards.

Knowing that pH was primarily maintained by the dissolution of CH and C-S-H from RCFs [38], finer particles clearly showed greater ability in constantly dissolving these two phases to compensate the OH^-. The significance of sustaining alkalinity during carbonation was closely associated with the speciation of dissolved CO_2 and the effect was illustrated in Fig. 16. It suggested that carbonate ions (i.e., CO_3^{2-}) were the dominant species over bicarbonate ions (HCO_3^-) and carbonic acid (H_2CO_3) at pH>10.5, while it totally disappeared at pH<7. Formation of the Cc was favourable with abundant CO_3^{2-} while it could become impossible with the absence of CO_3^{2-}. Therefore, the high pH environment at the starting stage was one of the critical factors responsible for quick Cc precipitation, and the longer alkalinity duration of RCF015 system contributed to longer Cc precipitation and thus the highest Cc amount. After the pH reached <7, carbonation was expected to suspend. However, it was experimentally observed to continue in the long run based on the Cc amount evolution as seen in Fig. 5. Considering the particle sizes, it was believed that carbonation in the bulk solution was suspended, but penetration of aqueous carbonate species (HCO_3^- and H_2CO_3) into the solid matrix became the main driven force for the ongoing carbonation.

The EC values, as monitored simultaneously with pH, also varied significantly depending on the particle size, with RCF015 system showing the highest conductivity and RCF236 the lowest (see Fig. 15b). It indicated that finer particles could release more ions than their coarse counterparts due to an enhanced dissolution. The trend of EC evolution could be described by a very rapid decrease at the initial stage and then a very slow increase afterwards. The time reaching the lowest EC values corresponded well with the time reaching pH=10.5, confirming the intensive reaction with the adequate presence of CO_3^{2-}. The rapid EC decrease was mainly ascribed to the consumption of Ca^{2+} to precipitate Cc, indicating the dissolution rate was much slower than its consumption. While at the later age, EC increase was due to the decreased carbonation rate, and the consumed ions were compensated by the diffusion of internally dissolved ions until an equilibrium.

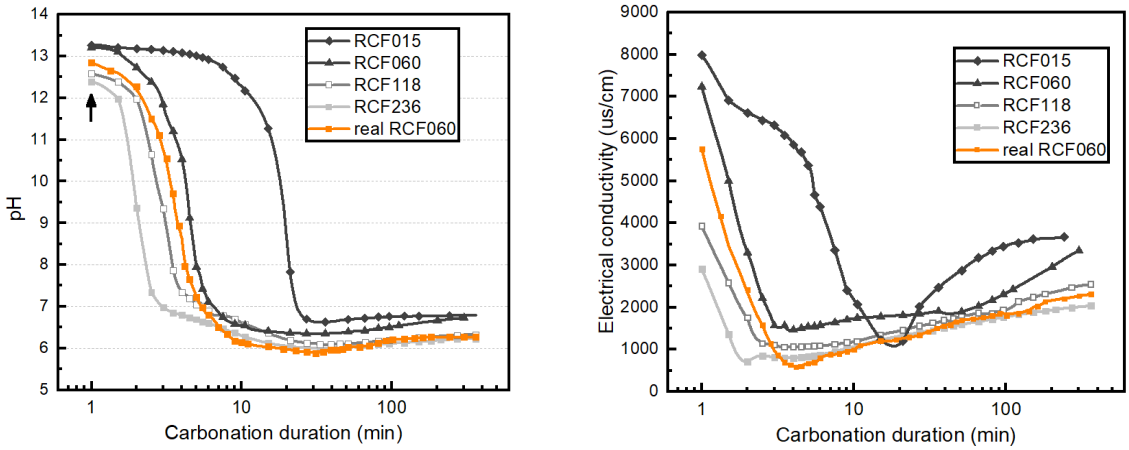

(a) (b)

422 Fig. 15. pH and EC evolution over time in the aqueous carbonation.

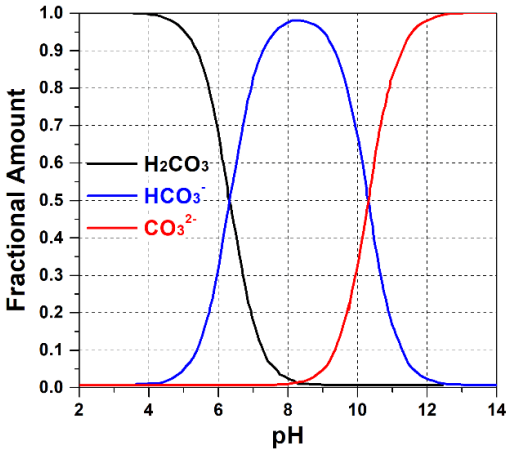

423

424 Fig. 16. Mole fractions of the carbonic acid, bicarbonate ions and carbonate ions as a function of pH
425 [46].

426 **3.3.2 Elemental concentrations**

427 As direct indicators of the AC reaction, elemental concentrations in the solution as determined by ICP-
428 OES are presented in Fig. 17. It was found that, prior to carbonation, Ca^{2+} was the predominant ion
429 dissolved from RCFs, the initial concentrations of which were 9.0, 11.6, 12.9 and 15.9 mM for RCF236,
430 RCF118, RCF060 and RCF015 respectively. The high Ca^{2+} concentration and the continuing
431 dissolution at the initial stage was the other reason for the intensive Cc precipitation apart from the
432 abundant CO_3^{2-}. Finer particles released more Ca^{2+} and thus contributed to higher EC values as
433 discussed above. Apart from the Ca^{2+}, alkali ions including the Na^+ and K^+ also showed high

concentrations but were rather varied among different particle sizes. It was observed that Na^+ concentration for RCF236 was only 1.0 mM, while it dramatically increased to about six times (i.e., 6.1 mM) for RCF015 due to the particle size reduction. K^+ behaved similarly and its concentration was 2.6 mM for RCF236 and increased to 7.3 mM for RCF015. Ca^{2+} originated from both the CH and C-S-H, while alkali ions were only from the C-S-H [47]. Therefore, the higher alkali concentration indicated a higher degree of C-S-H participating in the dissolution. The alkali concentrations reported in this study were similar to those in [25], both of which were clearly lower than the alkali concentrations in the common pore solutions of cement paste samples as reported by Lothenbach [48] and Vollpracht et al. [49] (typically ranged from 50 to 500mM). This was possibly owing to the dilution caused by the employment of a high liquid to solid ratio as well as the low amount of total alkalis in cement system as compared with Ca^{2+}, despite a high dissolution level of C-S-H in the late age of RCF015. In addition, it was observed that Ca^{2+} concentrations were about one to two orders of magnitude higher than Si, Al and S. The Si concentrations were found to be extremely low regardless of the particle size owing to the stable chain structure, while Al and S concentrations were slightly higher due to the dissolution of hydrated or anhydrous aluminate phases.

Upon the injection of CO_2, Ca^{2+} underwent the most significant consumption, as the concentrations were decreased by 10-21 times within just 1-2 min for RCF236, RCF118 and RCF060. As a comparison, the Ca^{2+} concentration reduction was much slower for RCF015, indicating a higher buffering ability. It was believed that the consumed Ca^{2+} could be rapidly compensated by the further dissolution of calcium-bearing phases in RCF015 on account of the fine particle size. However, after reaching the lowest point, the Ca^{2+} concentrations were found to slowly increase over time. This was because dissolution and reaction mainly occurred inside the RCF solid matrix and thus the concentration gradients were formed (higher in the solid matrix and lower in the bulk solution). As such, Ca^{2+} diffused back to the bulk solution until reaching an equilibrium.

The Na^+ and K^+ concentrations were relatively stable over time. This might be attributed to the high solubility of the alkalis and they were not precipitated as sole products. However, a decrease in K^+ for RCF015 and an increase of Na^+ and K^+ for RCF236 were also observed. The former might be due to the incorporation of K^+ into the carbonation product structure i.e., silica gel to obtain the charge balance, while the latter was attributed to the ongoing dissolution of C-S-H that released alkali ions. Besides, it

was seen that the S concentration of RCF015 was significantly higher than other RCFs. This was owing to the higher participation of aluminate phases in the dissolution and carbonation on account of the higher surface area. The alkali adsorption behavior of the carbonation-induced gel was also confirmed by Zajac et al. [50] through dosing external alkali solutions. It was found that higher concentrations of alkali solutions resulted in higher number of alkalis adsorptions in the gel, which subsequently led to the decrease in the position of Si–O bond vibration peak as well as the shift of ^{29}Si NMR resonance to higher frequency. Moreover, the higher alkali concentrations were also accompanied with enhanced sulphate leaching, which was also consistent with the observations in this study.

Realizing the above data was collected from paste RCFs to avoid huge variation from impurity contaminations, the behavior of real RCFs in the bulk solution was also determined as shown in Figs. 15 and 17 for comparison. The noticeable difference was the dilution effect caused by the incorporation of the inert phases (i.e., natural aggregate) since the results followed the same pattern of that of the paste RCFs. Thus, the behavior of real RCFs was consistent with the paste RCFs, which was reasonable since cement paste was the only reactive phase towards carbonation.

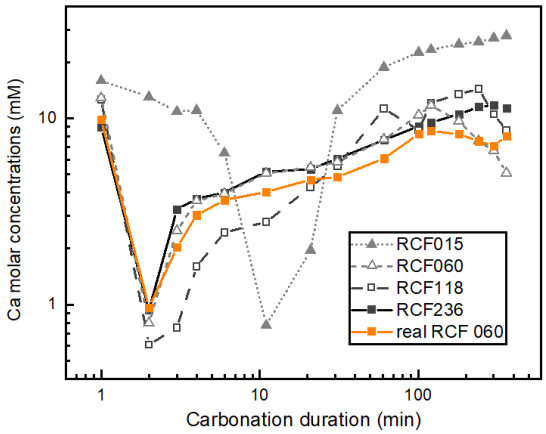

(a)

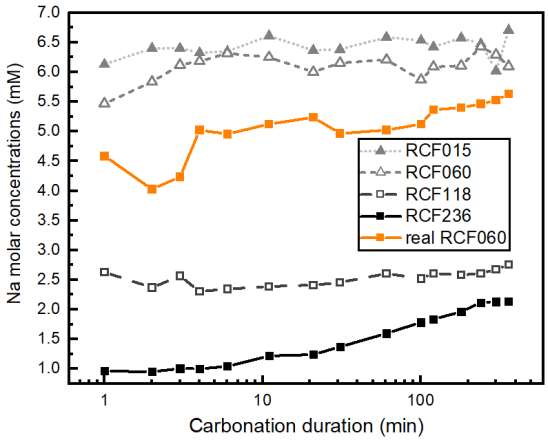

(b)

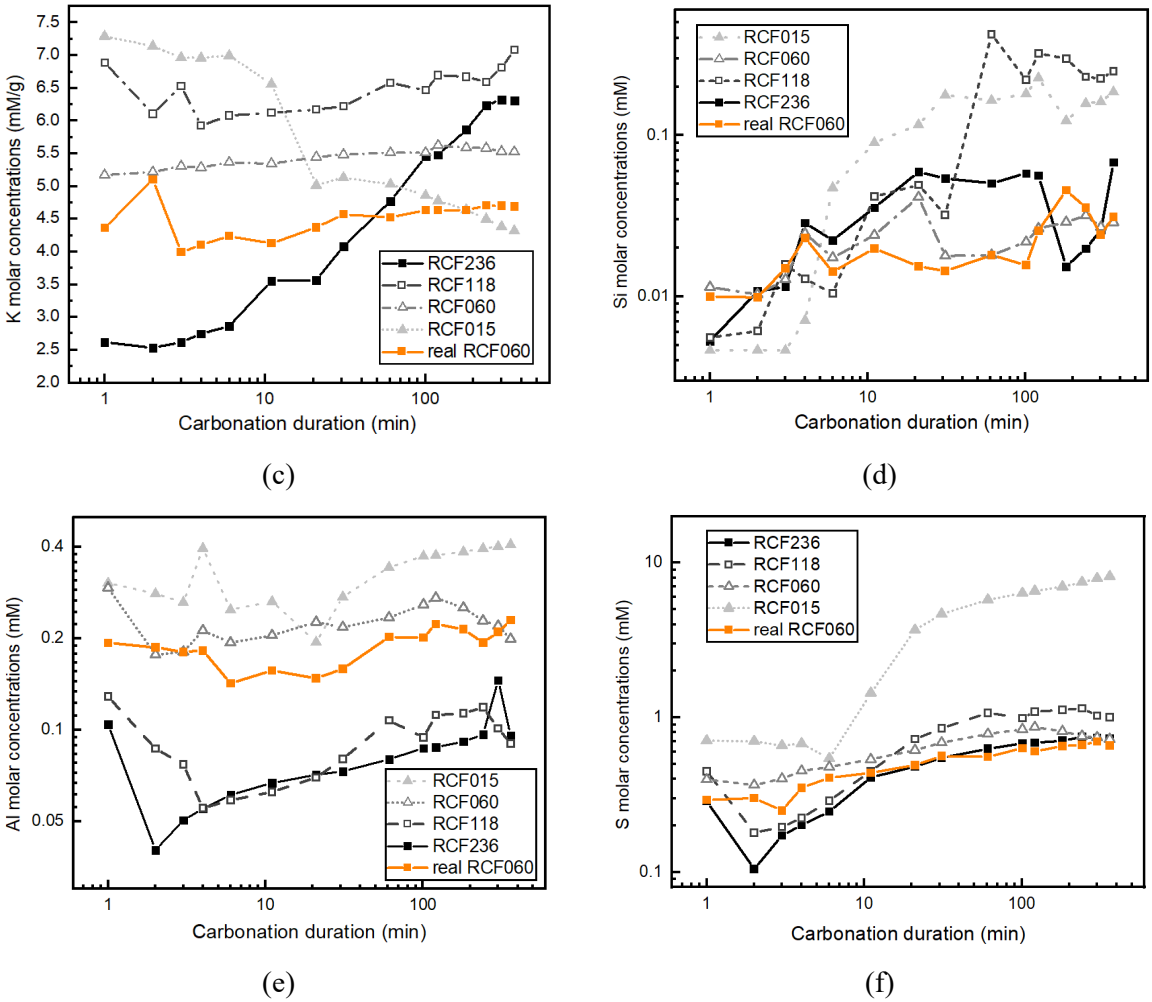

477 Fig. 17. Molar concentration evolution of (a) Ca, (b) Na, (c)K, (d)Si, (e) Al and (f) S in the solutions.

478

479 **3.4 Influence of AC on inert phases**

480 After validating the behaviour of real RCFs in bulk solution, the influence of AC on the inert phases
481 originally included in real RCFs was investigated via SEM. This was because the surface of the inert
482 phases (e.g., quartz or crushed granite) might be improved due to Cc deposition. As can be seen in Fig.
483 18a, in RCF015, quartz sand was mostly present as isolated particles, and they could be easily
484 recognized by their smooth surfaces. It was found these pure quartz particles were covered by extensive
485 amount of smaller grains. Based on the EDS spectra, the particle and the small grains were confirmed
486 as quartz and Cc respectively, confirming the deposition of Cc on inert phases. Besides, in the case of
487 RCF060 and RCF118, some quartz exposures could be observed; they were also partially covered by
488 the rhombohedral Cc. When the particle sizes further increased i.e., RCF236, larger quartz particle

surface could be seen (Fig. 18d). On these quartz surfaces, Cc precipitation could be clearly observed. Moreover, BSE images of the real RCFs were acquired with the EDS mapping. As shown in Fig. 19, a clear calcium-rich layer was observed around the quartz particle which was identified as the Cc deposition, thus suggesting a distinguished ability of AC in modifying the surface morphology of the inert phases. Cc has a higher affinity for Ca^{2+} than quartz sand; hence a higher density of C-S-H nuclei could form on the modified surface via the ionic-covalent bond, therefore improving the bonding when RCFs were used in new mortars [51].

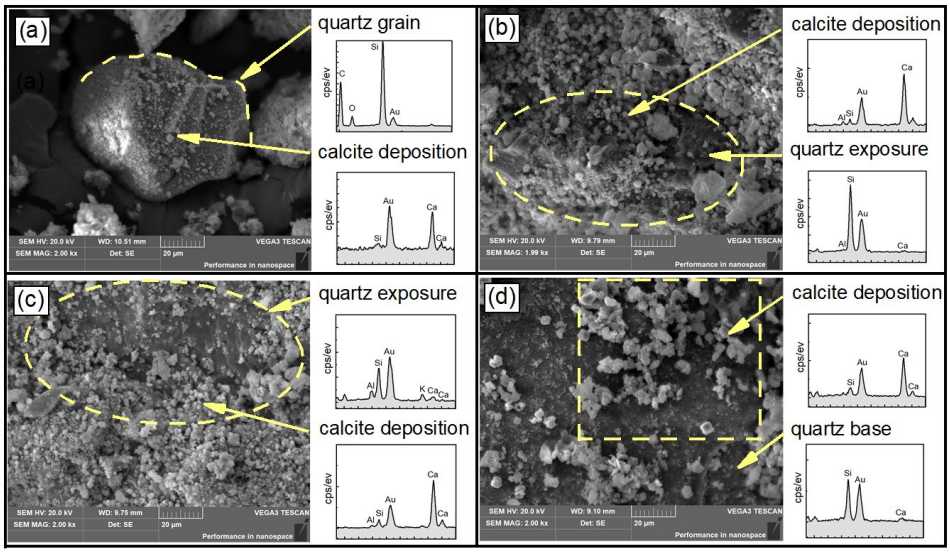

Fig. 18. SEM images of the quartz sand surface RCFs after aqueous carbonation (a) RCF015, (b) RCF060, (c) RCF118 and (d) RCF236.

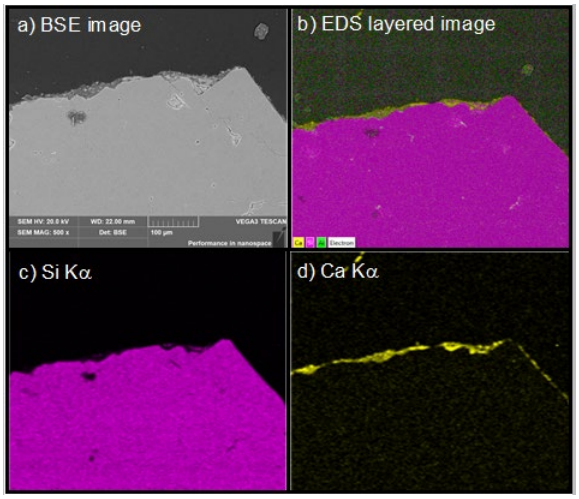

Fig. 19. Images of the inert quartz sand particle embedded in real RCF (a) BSE image, (b) EDS layered image, (c) Si Kα image and (d) Ca Kα image.

3.5 Influence of carbonated RCFs on compressive strength of pastes/mortars

RCF015 was carbonated for 6 h and used as cement replacement in new pastes. As shown in Fig. 20a, 65.7 MPa was attained for the pure OPC paste after hydration for 28 days. The use of 10% raw RCF015 in place of OPC resulted in a slight strength decrease to 62.0 MPa, while increasing dosages were found to result in up to 55.4% strength reduction, owing to poor reactivity of raw RCF015 and thus the dilution of OPC. As a comparison, the strength reduction was significantly mitigated with the use of carbonated RCF015. It was particularly obvious at the replacement level of 30%, which not only showed 13.2% improvement as compared with the raw RCF paste but also obtained an overall comparable strength to the pure OPC paste.

Meanwhile, to reflect the real applicability of RCF as fine aggregate, RCF060, RCF118 and RCF236 were mixed as per the grading curve similar to natural sand (Fig. 21) and then carbonated for 6 h. Subsequently, they were used as partial natural aggregate replacement (i.e., 20%, 40%, 60%) to make new mortars. The results (Fig. 20b) showed that the reference group with 100% natural sand achieved a compressive strength of 67.0 MPa at 28 days. While the use of 20% uncarbonated RCF resulted in 10.1% strength decrease to 60.2 MPa. Besides, the strength was found to be further decreased with the increasing amount of uncarbonated RCF, to a lowest of 54.6 MPa at 60%, suggesting a 18.5% reduction. This monotonous strength reduction was owing to the high porosity of RCF and the weak interfacial transition zone in new mortar when compared with natural aggregate as well documented in previous studies [1, 52]. However, when carbonated RCF was used, strength decrease was also significantly mitigated. The mortar with 20% carbonated RCF achieved comparable strength to the reference (i.e., 65.7 MPa), and the mortar made with 60% carbonated RCF still attained 58.5 MPa. Therefore, the AC was found to be an efficient and effective method to treat the RCFs and to improve their performance as SCM or aggregates.

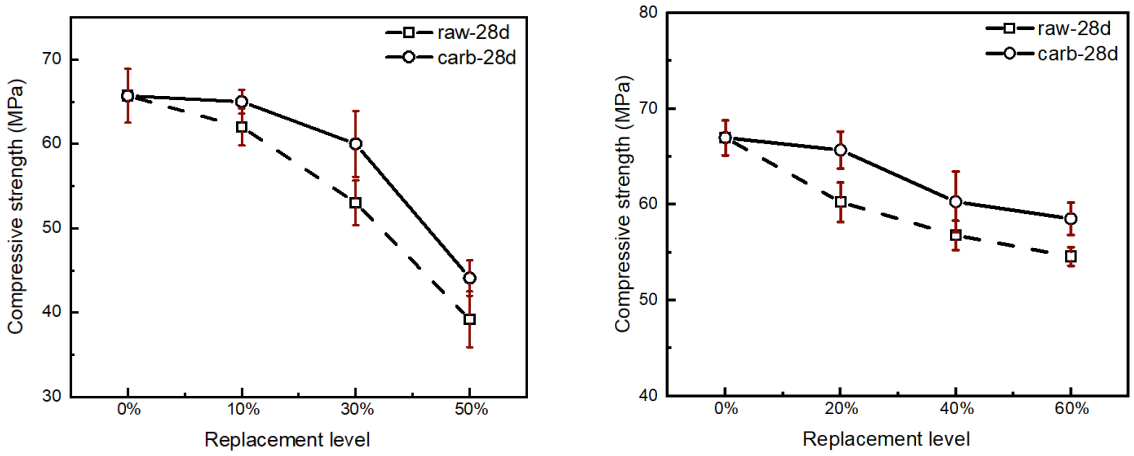

527 Fig. 20. Compressive strength development of (a) pastes containing RCF015 and (b) mortars
528 containing RCF060-236.

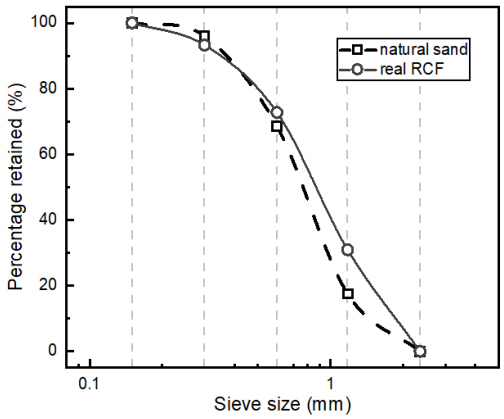

529

530 Fig. 21. Grading curves of the natural quartz sand and the combined real RCFs used in mortar.

531

532 **4 Summary and discussion**

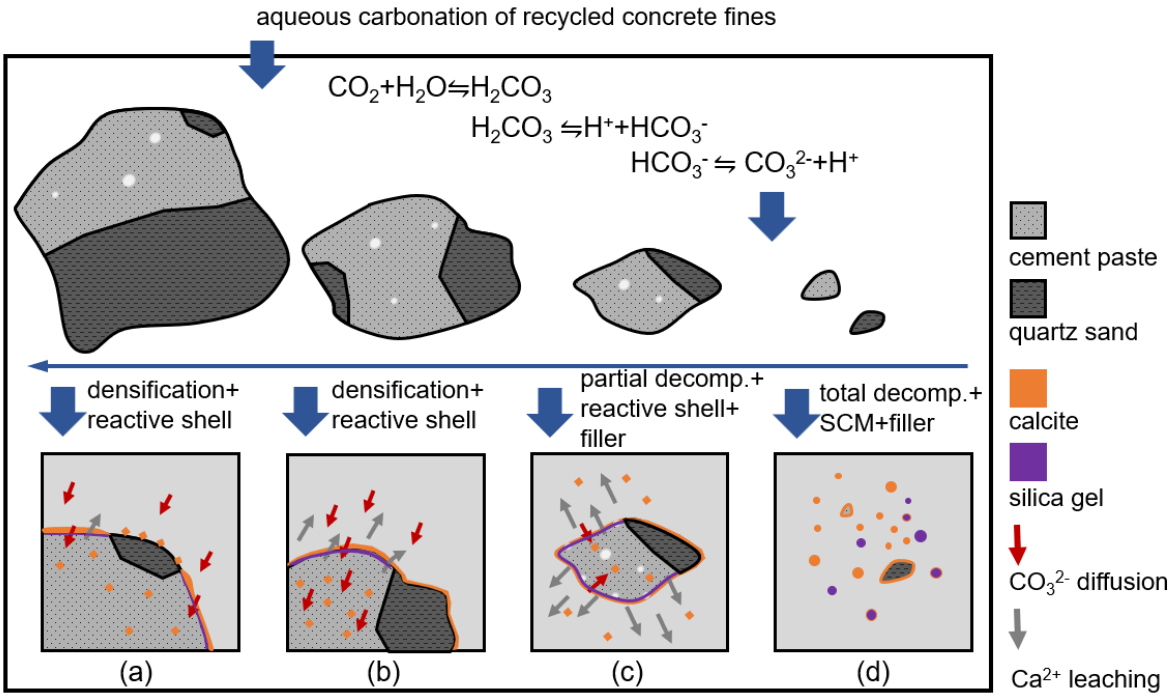

Fig. 22. Illustration of the reaction process of aqueous carbonation on recycled concrete fines (a) RCF236, (b) RCF118, (c) RCF060 and (d) RCF015.

As presented above, the RCFs subjected to AC were modified differently depending on the particle sizes. As illustrated in Fig. 22, the largest particle RCF236 formed a dense and reactive shell on its surface. The shell contained pure Cc coating and thoroughly decalcified silica gel (Q^4). In addition to the shell, RCF236 also underwent significant pore refinement after AC, leading to the densification of its solid matrix. RCF118, as slightly finer than RCF236, exhibited a similar shell formation and densification effects. By contrast, RCF060 was reckoned as the transition group because it encountered partial decomposition firstly and then densification in the long run. Overall, it released Cc from its main matrix, formed a reactive shell and generated a higher amount of total silica gel (Q^3+Q^4) and Cc was also formed away from its main matrix. With the further decrease of particle size (i.e., RCF015), drastic decomposition occurred, and the powder was almost totally converted to a Cc and silica gel composite, accompanied by the disintegration of the solid matrix.

The significantly different responses of RCFs upon carbonation were related to the different CO_2-water-RCFs interactions. Dissolution and leaching, which naturally took place when the RCFs were immersed in water, were the very first step of the liquid-solid reaction. It referred to i) the hydrolysis of calcium-

bearing phases, and ii) the diffusion of Ca^{2+} from the solid into the solution, which resulted in the increase of alkalinity, conductivity and Ca^{2+} concentrations. The high alkalinity maintained the carbonate species in the form of CO_3^{2-} when CO_2 was ionized. As such, the newly formed CO_3^{2-} upon injection of gaseous CO_2 could immediately react with the readily dissolved Ca^{2+} in the solution. Therefore, the solution became quickly oversaturated with respect to Cc [39, 40] and thus it intensively nucleated and precipitated on the unreacted surface of RCFs, thus forming the Cc coating. However, as shown in Fig. 15a and 17a, due to the fine particle size, RCF015 dissolved more quickly and thus showed a higher ability in buffering the alkalinity and Ca^{2+} concentrations in the solution. Therefore, the Cc precipitation lasted much longer, causing its total decomposition. On the other hand, the recovery of pH and Ca^{2+} from the coarse particles (RCF060, RCF118 and RCF236) was slower and thus the high alkalinity period was quickly ended. Subsequently, the carbonate species diffused through the pores into the alkaline solid matrix [30] and reacted with the inner Ca^{2+} to precipitate Cc, resulting in the densification of the matrix.

Besides, it was highlighted in Fig. 5 that the formation of Cc was quite intensive, as 68-88% of the final amount of Cc was formed within 30 min. However, extending carbonation duration was meaningful in obtaining i) more silica gel for RCF015 and RCF060, and ii) more densified structure for RCF118 and RCF236. They contributed differently to the development of compressive strength when used in pastes/mortars. For RCF015, it mainly played the role of SCM where extensive amounts of Cc and silica gel were present. The micro-sized Cc not only acted as micro-fillers in the blended cement paste, but also reacted with the aluminate phase and stabilized the ettringite; while the silica gel was reacted with CH to produce additional C-S-H [53]. For RCF236 and RCF118, they could provide a stronger framework for the mortar to attain higher strength; meanwhile, as revealed by our previous study, the reactive shell formed helped to develop a better bonding between the RCFs with the new cement mortar [40, 53], and thus an enhanced interfacial transition zone [26, 53]. Nevertheless, the RCF060 fraction in the aggregates could act as a smart aggregate that not only provided more silica gel and Cc coating to trigger the pozzolanic reaction and enhance bonding, but also some Cc were decomposed from its main body as micro- or nano-fillers for the mortar (see Fig. 13b).

5 Conclusions

580 This study investigated the effects of AC on different fractions of RCFs. Characteristic changes in the
581 cement paste, inert phase, bulk solutions and their influences in compressive strength development of
582 new paste (as cement substitutes) and mortars (as fine aggregate substitutes) were investigated. By
583 reviewing the experimental results presented above, the following conclusions can be drawn:

584 (1) AC was very efficient in carbonating the RCFs, about 68-88% of the final amount of Cc was formed
585 within 30 min. Nevertheless, the total amount of Cc precipitation was dependent on particle size, with
586 the fractions RCF015, RCF060, RCF118 and RCF236 possessing 70.7%, 21.5%, 14.2% and 9.0% Cc
587 respectively after carbonation for 6h.The precipitated Cc was found to be well-crystallized calcite,
588 showing rhombohedral morphology. No presence of aragonite and vaterite was detected.

589 (2) Unlike the quick precipitation of Cc, silica gel was progressively formed mainly in the late period
590 (>1h). Approximately 70% of silicate phases were polymerized into silica gel after 6h with regard to
591 RCF015. Increasing the particle size significantly decreased the amount of silica gel to 17.1%, 11.7%
592 and 7.3% for RCF060, RCF118 and RCF236 respectively.

593 (3) The pore structure of the carbonated RCFs also showed a strong particle size effect. Extensive gel
594 pores were formed in RCF015 associated with the formation of silica gel, resulting in the increase of
595 cumulative pore volume by about 70%. As a comparison, the RCF118 and RCF236 had decreased pore
596 volume by up to 31%, indicative of structural densification. RCF060 was a transition where dissolution-
597 induced pore coarsening occurred in the initial period and densification took place in the later period.

598 (4) Modification of AC on the microstructure of RCFs was firstly surface-based when the
599 dissolution/decalcification took place mainly on the surface layers. It was responsible for the formation
600 of the shell-core structure where the Cc coating and silica gel layer formed the shell. However, it
601 gradually became diffusion controlled by the internal diffusion of aqueous carbonate species, thus
602 leading to the densification of RCF matrices, which was referred to as the densified core. While for
603 decreased particle size e.g., RCF015, Cc not only precipitated on the surface of the particles but also
604 massively nucleated and grew in the solution space, thus causing its disintegration and decomposition.

605 (5) From the solution chemistry point of view, the strong alkalinity maintaining and Ca^{2+} buffering
606 ability of RCF015 on account of its fine particle size was the primary reason why RCF015 was totally
607 decomposed. Specifically, the high alkalinity favored CO_2 dissolution and CO_3^{2-} availability, while the

608 consumption of Ca^{2+} was quickly buffered by the dissolution of calcium-bearing phases. In this manner,
609 the RCF015 was significantly reacted. Nevertheless, the carbonation of RCF236 and RCF118 mediated
610 in the bulk solution was quickly suspended due to the quick lowering of pH and was subsequently
611 slowly driven by the inward penetration of aqueous carbonate species into the solid matrix where local
612 environment was alkaline.

613 (6) Overall, the quality of RCF236 and RCF118 was improved after AC by densifying the solid matrices
614 and improving the surface properties with a higher bonding ability. Meanwhile, the quality of the
615 RCF060 was improved due to the partial decomposition, formation of abundant amounts of Cc and
616 silica gel. In contrast, the quality of RCF015 was improved by significantly modifying its composition
617 and reactivating its cementing ability. Besides, the inert phases embedded in RCFs were found to have
618 some Cc depositions due to the characteristic dissolution and precipitation process of AC. Therefore,
619 when incorporating the carbonated RCFs into mortars as aggregates or into cement paste as a SCM, the
620 compressive strength was markedly improved.

621

622 **Acknowledgement**

623 The authors wish to thank the Hong Kong Construction Industry Council (CICR/03/19) and the
624 Research Grants Council GRF (PolyU 152144/17E) for financial support.

625

626 **References**

627 [1] K.P. Verian, W. Ashraf, Y. Cao, Properties of recycled concrete aggregate and their influence in
628 new concrete production, Resources, Conservation and Recycling, 133 (2018) 30-49.
629 [2] H. Guo, C. Shi, X. Guan, J. Zhu, Y. Ding, T.-C. Ling, H. Zhang, Y. Wang, Durability of recycled
630 aggregate concrete – A review, Cement and Concrete Composites, 89 (2018) 251-259.
631 [3] F. López-Gayarre, P. Serna, A. Domingo-Cabo, M.A. Serrano-López, C. López-Colina, Influence
632 of recycled aggregate quality and proportioning criteria on recycled concrete properties, Waste
633 Management, 29 (2009) 3022-3028.
634 [4] P. Belin, G. Habert, M. Thiery, N. Roussel, Cement paste content and water absorption of recycled
635 concrete coarse aggregates, Materials and Structures, 47 (2014) 1451-1465.
636 [5] X. Fang, D. Xuan, C.S. Poon, Empirical modelling of CO2 uptake by recycled concrete aggregates
637 under accelerated carbonation conditions, Materials and Structures, 50 (2017).

[6] J. Xiao, Z. Ma, T. Sui, A. Akbarnezhad, Z. Duan, Mechanical properties of concrete mixed with recycled powder produced from construction and demolition waste, Journal of Cleaner Production, 188 (2018) 720-731.
[7] S. Li, J. Gao, Q. Li, X. Zhao, Investigation of using recycled powder from the preparation of recycled aggregate as a supplementary cementitious material, Construction and Building Materials, 267 (2021) 120976.
[8] L. Oksri-Nelfia, P.Y. Mahieux, O. Amiri, P. Turcry, J. Lux, Reuse of recycled crushed concrete fines as mineral addition in cementitious materials, Materials and Structures, 49 (2015) 3239-3251.
[9] C. Shi, Y. Li, J. Zhang, W. Li, L. Chong, Z. Xie, Performance enhancement of recycled concrete aggregate – A review, Journal of Cleaner Production, 112 (2016) 466-472.
[10] V.W.Y. Tam, H. Wattage, K.N. Le, A. Buteraa, M. Soomro, Methods to improve microstructural properties of recycled concrete aggregate: A critical review, Construction and Building Materials, 270 (2021).
[11] A. Gholizadeh-Vayghan, A. Bellinkx, R. Snellings, B. Vandoren, M. Quaghebeur, The effects of carbonation conditions on the physical and microstructural properties of recycled concrete coarse aggregates, Construction and Building Materials, 257 (2020) 119486.
[12] B. Lu, C. Shi, Z. Cao, M. Guo, J. Zheng, Effect of carbonated coarse recycled concrete aggregate on the properties and microstructure of recycled concrete, Journal of Cleaner Production, 233 (2019) 421-428.
[13] D. Xuan, B. Zhan, C.S. Poon, Assessment of mechanical properties of concrete incorporating carbonated recycled concrete aggregates, Cement and Concrete Composites, 65 (2016) 67-74.
[14] B.J. Zhan, D.X. Xuan, W. Zeng, C.S. Poon, Carbonation treatment of recycled concrete aggregate: Effect on transport properties and steel corrosion of recycled aggregate concrete, Cement and Concrete Composites, 104 (2019) 103360.
[15] G. Chinzorigt, M.K. Lim, M. Yu, H. Lee, O. Enkbold, D. Choi, Strength, shrinkage and creep and durability aspects of concrete including CO2 treated recycled fine aggregate, Cement and Concrete Research, 136 (2020) 106062.
[16] J. Zhang, C. Shi, Y. Li, X. Pan, C.-S. Poon, Z. Xie, Performance Enhancement of Recycled Concrete Aggregates through Carbonation, Journal of Materials in Civil Engineering, 27 (2015) 04015029.
[17] C. Liang, H. Ma, Y. Pan, Z. Ma, Z. Duan, Z. He, Chloride permeability and the caused steel corrosion in the concrete with carbonated recycled aggregate, Construction and Building Materials, 218 (2019) 506-518.
[18] B. Lu, C. Shi, J. Zhang, J. Wang, Effects of carbonated hardened cement paste powder on hydration and microstructure of Portland cement, Construction and Building Materials, 186 (2018) 699-708.
[19] X. Ouyang, L. Wang, S. Xu, Y. Ma, G. Ye, Surface characterization of carbonated recycled concrete fines and its effect on the rheology, hydration and strength development of cement paste, Cement and Concrete Composites, 114 (2020) 103809.
[20] E. Kangni-Foli, S. Poyet, P. Le Bescop, T. Charpentier, F. Bernachy-Barbé, A. Dauzères, E. L'Hôpital, J.B. D'Espinose De Lacaillerie, Carbonation of model cement pastes: The mineralogical origin of microstructural changes and shrinkage, Cement and Concrete Research, 144 (2021) 106446.
[21] K. De Weerdt, M.B. Haha, G. Le Saout, K.O. Kjellsen, H. Justnes, B. Lothenbach, Hydration mechanisms of ternary Portland cements containing limestone powder and fly ash, Cement and Concrete Research, 41 (2011) 279-291.

[22] B.J. Zhan, C.S. Poon, C.J. Shi, Materials characteristics affecting CO2 curing of concrete blocks containing recycled aggregates, Cement and Concrete Composites, 67 (2016) 50-59.
[23] G.H.D. Tonoli, G.F. Carmello, C.A. Fioroni, T.D.L. Pereira, G. Rocha, R.B.D. Souza, V.M. John, H. Savastano, Influence of the initial moisture content on the carbonation degree and performance of fiber-cement composites, Construction and Building Materials, 215 (2019) 22-29.
[24] C. Shi, F. He, Y. Wu, Effect of pre-conditioning on CO2 curing of lightweight concrete blocks mixtures, Construction and Building Materials, 26 (2012) 257-267.
[25] M. Zajac, J. Skibsted, J. Skocek, P. Durdzinski, F. Bullerjahn, M. Ben Haha, Phase assemblage and microstructure of cement paste subjected to enforced, wet carbonation, Cement and Concrete Research, 130 (2020) 105990.
[26] S. Liu, P. Shen, D. Xuan, L. Li, A. Sojobi, B. Zhan, C.S. Poon, A comparison of liquid-solid and gas-solid accelerated carbonation for enhancement of recycled concrete aggregate, Cement and Concrete Composites, 118 (2021) 103988.
[27] H.J. Ho, A. Iizuka, E. Shibata, H. Tomita, K. Takano, T. Endo, CO2 Utilization via Direct Aqueous Carbonation of Synthesized Concrete Fines under Atmospheric Pressure, ACS Omega, 5 (2020) 15877-15890.
[28] S. Kashef-Haghighi, S. Ghoshal, Physico–Chemical Processes Limiting CO2 Uptake in Concrete during Accelerated Carbonation Curing, Industrial & Engineering Chemistry Research, 52 (2013) 5529-5537.
[29] A. Ben Ghacham, E. Cecchi, L.C. Pasquier, J.F. Blais, G. Mercier, CO2 sequestration using waste concrete and anorthosite tailings by direct mineral carbonation in gas-solid-liquid and gas-solid routes, J Environ Manage, 163 (2015) 70-77.
[30] F. Faraji, A. Alizadeh, F. Rashchi, N. Mostoufi, Kinetics of leaching: a review, Reviews in Chemical Engineering, 38 (2020) 113-148.
[31] H.-J. Ho, A. Iizuka, E. Shibata, Chemical recycling and use of various types of concrete waste: A review, Journal of Cleaner Production, 284 (2021).
[32] P. Shen, Y. Sun, S. Liu, Y. Jiang, H. Zheng, D. Xuan, J. Lu, C.S. Poon, Synthesis of amorphous nano-silica from recycled concrete fines by two-step wet carbonation, Cement and Concrete Research, 147 (2021) 106526.
[33] V.W.Y. Tam, M. Soomro, A.C.J. Evangelista, Quality improvement of recycled concrete aggregate by removal of residual mortar: A comprehensive review of approaches adopted, Construction and Building Materials, 288 (2021) 123066.
[34] V.W.Y. Tam, C.M. Tam, K.N. Le, Removal of cement mortar remains from recycled aggregate using pre-soaking approaches, Resources, Conservation and Recycling, 50 (2007) 82-101.
[35] K. Scrivener, R. Snellings, B. Lothenbach, A practical guide to microstructural analysis of cementitious materials, Crc Press2018.
[36] Y.A. Villagrán-Zaccardi, H. Egüez-Alava, K. De Buysser, E. Gruyaert, N. De Belie, Calibrated quantitative thermogravimetric analysis for the determination of portlandite and calcite content in hydrated cementitious systems, Materials and Structures, 50 (2017).
[37] M. Zajac, A. Rossberg, G. Le Saout, B. Lothenbach, Influence of limestone and anhydrite on the hydration of Portland cements, Cement and Concrete Composites, 46 (2014) 99-108.
[38] Z. Shi, B. Lothenbach, M.R. Geiker, J. Kaufmann, A. Leemann, S. Ferreiro, J. Skibsted, Experimental studies and thermodynamic modeling of the carbonation of Portland cement, metakaolin and limestone mortars, Cement and Concrete Research, 88 (2016) 60-72.

[39] M. Zajac, J. Skibsted, P. Durdzinski, F. Bullerjahn, J. Skocek, M. Ben Haha, Kinetics of enforced carbonation of cement paste, Cement and Concrete Research, 131 (2020) 106013.
[40] Y. Jiang, P. Shen, C.s. Poon, Improving the bonding capacity of recycled concrete aggregate by creating a reactive shell with aqueous carbonation, Construction and Building Materials, 315 (2021) 125733.
[41] B. Walkley, J.L. Provis, Solid-state nuclear magnetic resonance spectroscopy of cements, Materials Today Advances, 1 (2019) 100007.
[42] J.J. Chen, J.J. Thomas, H.M. Jennings, Decalcification shrinkage of cement paste, Cement and Concrete Research, 36 (2006) 801-809.
[43] M. Castellote, C. Andrade, X. Turrillas, J. Campo, G.J. Cuello, Accelerated carbonation of cement pastes in situ monitored by neutron diffraction, Cement and Concrete Research, 38 (2008) 1365-1373.
[44] W. Ashraf, J. Olek, Elucidating the accelerated carbonation products of calcium silicates using multi-technique approach, Journal of CO2 Utilization, 23 (2018) 61-74.
[45] B. Wu, G. Ye, Development of porosity of cement paste blended with supplementary cementitious materials after carbonation, Construction and Building Materials, 145 (2017) 52-61.
[46] C. Kim, J. Kim, S. Joo, Y. Bu, M. Liu, J. Cho, G. Kim, Efficient CO2 Utilization via a Hybrid Na-CO2 System Based on CO2 Dissolution, iScience, 9 (2018) 278-285.
[47] Y. Yan, S.-Y. Yang, G.D. Miron, I.E. Collings, E. L'Hôpital, J. Skibsted, F. Winnefeld, K. Scrivener, B. Lothenbach, Effect of alkali hydroxide on calcium silicate hydrate (C-S-H), Cement and Concrete Research, 151 (2022) 106636.
[48] B. Lothenbach, Thermodynamic equilibrium calculations in cementitious systems, Materials and Structures, 43 (2010) 1413-1433.
[49] A. Vollpracht, B. Lothenbach, R. Snellings, J. Haufe, The pore solution of blended cements: a review, Materials and Structures, 49 (2015) 3341-3367.
[50] M. Zajac, J. Skibsted, P. Durdzinski, M. Ben Haha, Effect of alkalis on products of enforced carbonation of cement paste, Construction and Building Materials, 291 (2021) 123203.
[51] X. Ouyang, D.A. Koleva, G. Ye, K. Van Breugel, Understanding the adhesion mechanisms between C S H and fillers, Cement and Concrete Research, 100 (2017) 275-283.
[52] M.S. de Juan, P.A. Gutiérrez, Study on the influence of attached mortar content on the properties of recycled concrete aggregate, Construction and Building Materials, 23 (2009) 872-877.
[53] B.J. Zhan, D.X. Xuan, C.S. Poon, K.L. Scrivener, Characterization of interfacial transition zone in concrete prepared with carbonated modeled recycled concrete aggregates, Cement and Concrete Research, 136 (2020) 106175.